Nanoscale

PAPER

View Article Online
View Journal | View Issue

Cite this: *Nanoscale*, 2017, **9**, 7941

Employing shells to eliminate concentration quenching in photonic upconversion nanostructure†

Jing Zuo,[a,b,c] Qiqing Li,[a,b] Bin Xue,[a,c] Cuixia Li,[a] Yulei Chang,[a] Youlin Zhang,[a] Xiaomin Liu,[a] Langping Tu,*[a,c] Hong Zhang [c] and Xianggui Kong *[a]

Received 25th February 2017,
Accepted 21st May 2017

DOI: 10.1039/c7nr01403a

rsc.li/nanoscale

It is generally accepted that a lanthanide ions based upconversion material follows an activator low doping strategy (normally <3 mol%), because of the restriction of the harmful concentration quenching effect. Here, we demonstrate that this limitation can be broken in nanostructures. Simply by using an inert shell coating strategy, the concentration quenching effect for the activator (Er^{3+}) could be eliminated and highly efficient upconversion luminescence realized in the activator fully doped nanostructure, *e.g.* $NaErF_4$@$NaYF_4$. More importantly, this novel nanostructure achieves some long-cherished desires, such as multiple-band co-excitation (~800 nm, ~980 nm and ~1530 nm) and monochromic red emission. Proof-of-concept experiments are presented of the potential benefit of this structure in solar cells and anti-counterfeiting. This nanostructure offers new possibilities in realizing high upconversion emission and novel functionalities of lanthanide based nanomaterials.

1. Introduction

Since the mid-1960s, lanthanide ion (Ln^{3+}) doped materials have displayed attractive potentiality in numerous fields (solar cells, biology, displays and security *etc.*),[1–12] due to their unique luminescent property of converting near-infrared (NIR) excitation to ultraviolet (UV) or visible (VIS) light emission. For this material, one of the most important issues is to identify the optimal host-dopant combinations to obtain highly efficient upconversion (UC) emission. To date, almost all the efficient UC systems adopt the sensitizer/activator co-doping strategy, and usually the doping concentration of the activator remains at a low level (*e.g.* below 3 mol%).[13,14] This status is mainly attributed to the following inherent points of view. Over the years, it has generally been believed that it is difficult to observe efficient UC emission without the help of sensitizer ions (*e.g.* Yb^{3+}, Nd^{3+}), due to the limitation of the insufficient absorption ability of the activator. In the meantime, the compensation method for this issue, *i.e.* raising the concentration of the activator, is considered likely to trigger the negative concentration quenching effect (the high doping concentration will lead to harmful cascade energy migration and cross-relaxation between dopant ions, thus increasing the probability for excited state energy to be trapped by the quenching sites).[15] Until now, only limited improvements have been made in suppressing the concentration quenching effect, such as the spatial doping strategy,[16–18] forming ion clusters in the nanostructure[19] and utilizing ultra-high excitation irradiance (10^6 W cm^{-2}).[20,21] However, the fundamental issues to further improve the optimal concentration of activator remain far from resolved. The relevant mechanism is still puzzling. And in practice, under the traditional low excitation irradiance (<10^3 W cm^{-2}), the UC efficiency for activator heavily-doped nanosystems is still at least one order of magnitude lower than that of the widely accepted activator low-doping systems (*e.g.* $NaYF_4$:20% Yb,2% Er@$NaYF_4$, upon excitation of 980 nm).[22,23]

Herein, we report an efficient core-inert shell UC nanostructure with a strongly suppressed concentration quenching effect of the activator (Er^{3+}) in the luminescent core area, for which the optimal doping concentration of Er^{3+} in the core can reach up to 100 mol%. Interestingly, this activator "fully-doped" core-inert shell nanostructure, *i.e.* $NaErF_4$@$NaYF_4$ and its relevant derivatives (*e.g.* $NaErF_4$:0.5% Tm@$NaYF_4$), exhibit many unique UC properties, such as high luminescent efficiency, multi-band excitation in the NIR region (~800 nm, ~980 nm, ~1530 nm) and monochromic red emission (~650 nm). By studying a series of steady-state and time-resolved spectroscopic experimental results, the suppression of the concentration quenching effect is certified to come from

[a]State Key Laboratory of Luminescence and Applications, Changchun Institute of Optics, Fine Mechanics and Physics, Chinese Academy of Sciences, Changchun 130033, China. E-mail: xgkong14@ciomp.ac.cn, tulangping@163.com
[b]Graduate University of the Chinese Academy of Sciences, Beijing 100049, China
[c]Van' t Hoff Institute for Molecular Sciences, University of Amsterdam, Science Park 904, 1098 XH Amsterdam, The Netherlands

†Electronic supplementary information (ESI) available. See DOI: 10.1039/c7nr01403a

the "quenching site free" environment of the activator, which brings us a new understanding of the concentration quenching mechanism. Furthermore, the advantages of this multi-band excitable UC structure in potential applications like solar cells and anti-counterfeiting have been proved by proof-of-concept experiments.

2. Experimental section

2.1 Reagents

$LnCl_3{\cdot}6H_2O$ (Ln: Y, Yb, Er >99%), Ln_2O_3 (Ln: Y, Yb, Er, Nd >99%), oleic acid (OA, 90%), 1-octadecene (ODE, 90%), oleylamine (OM, 90%), sodium trifluoroacetate (98%) and trifluoroacetic acid (99%) were purchased from Sigma-Aldrich and used without further purification. NaOH (>98%), NH_4F (>98%), methanol, ethanol and cyclohexane were purchased from GFS Chemical.

2.2 Synthesis of 20 nm β-$NaYF_4$:20% Yb,2% Er and 20 nm β-$NaYF_4$:*x*% Er (*x*: 2–100) bare core nanoparticles

The 20 nm β-$NaYF_4$:Yb,Er nanoparticles and 20 nm β-$NaYF_4$:*x*% Er (*x*: 2–100) nanoparticles were synthesized following a previous approach in the literature.[24]

2.3 Synthesis of the β-core–shell nanoparticles

The $NaYF_4$:20% Yb,2% Er@$NaYF_4$, $NaYF_4$:*x*% Er@$NaYF_4$ (*x*: 2–100), $NaErF_4$:0.5% Tm@$NaYF_4$ and $NaYF_4$:20% Yb,2% Er@$NaYF_4$:20%Yb@$NaYF_4$:10% Nd core–shell (or core–shell–shell) nanoparticles were prepared following a previous approach in the literature.[25]

2.4 Characterization

The structure and morphology of the nanoparticles were characterized by using a Bruker D8-advance X-ray diffractometer (XRD) with Cu Kα radiation (λ = 1.5418 Å). Transmission electron microscopy (TEM) was performed on a Tecnai G2 F20 S-TWIN D573 electron microscope operated at 300 kV TEM. Ultraviolet-visible (UV) absorption measurements were recorded using a UV-3101 spectrophotometer. The upconversion emission spectra were measured at room temperature by a Maya 2000 visible spectrometer (Ocean optics). The luminescent dynamics were recorded with a 500 MHz Tektronix digital oscilloscope and the excitation was realized by a nanosecond pulse train at 800 nm, 980 nm and 1530 nm from an optical parametric oscillator.

3. Results and discussion

The core–shell nanoparticles were synthesized through a typical procedure.[25] Taking $NaErF_4$@$NaYF_4$ as an example, the uniform size and morphology of the nanoparticles before and after shell coating are revealed by low-resolution transmission electron microscopy (TEM) imaging (Fig. 1a and b). The diameters of the core and core–shell nanoparticle were confirmed

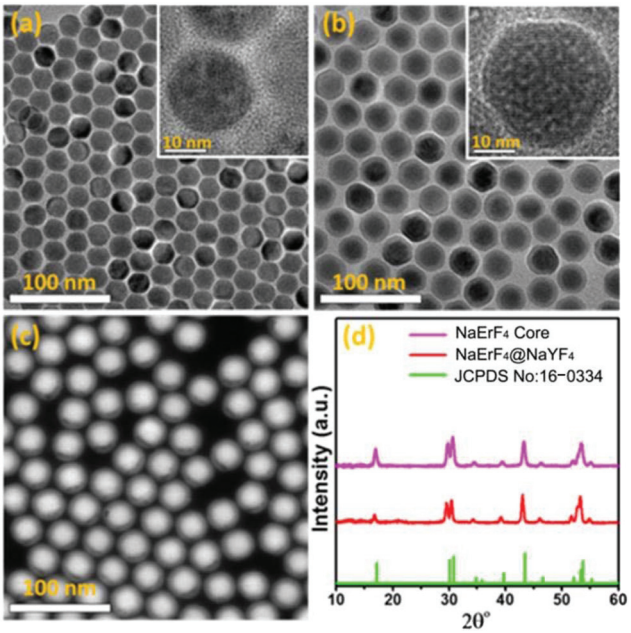

Fig. 1 Structure characterization of $NaErF_4$ and $NaErF_4$@$NaYF_4$ nanoparticles. The low-resolution TEM and high-resolution TEM (inset) images of (a) the $NaErF_4$ bare core nanoparticles, (b) the as-prepared $NaErF_4$@$NaYF_4$ core–shell nanoparticles. (c) Typical high angle annular dark field (HAADF) image of the $NaErF_4$@$NaYF_4$ core–shell nanoparticle. (d) Corresponding powder XRD diffraction patterns of the $NaErF_4$ and $NaErF_4$@$NaYF_4$ nanoparticles; contrast with the standard hexagonal structure of $NaYF_4$ nanoparticles.

as 20 ± 1.5 nm and 30 ± 2 nm, respectively, as shown in the high-resolution TEM imaging (Fig. 1a and b insets). The shell thickness (5 nm) was verified by the high angle annular dark field (HAADF) image (Fig. 1c). And the Er^{3+} dopant concentrations are confirmed by the element analysis results (refer to the ESI Fig. S1†). In addition, the crystal structures of $NaErF_4$ bare core and $NaErF_4$@$NaYF_4$ core–shell were confirmed as a pure hexagonal-phase structure by X-ray powder diffraction (XRD) results, as shown in Fig. 1d (contrast with the standard hexagonal structure of $NaYF_4$ nanoparticles, Joint Committee on Powder Diffraction Standards file number 16-0334).‡

Unlike the traditional sensitizer-activator co-doping systems, which usually only work effectively on one specific excitation wavelength (*e.g.* ~800 nm, ~980 nm or ~1530 nm), because of the unique ladder-like energy levels of Er^{3+},[26] the $NaErF_4$@$NaYF_4$ core–shell nanostructure has the ability to obtain efficient UC emission under all of the three excitation models mentioned above. To evaluate its UC properties, comparisons have been conducted between $NaErF_4$@$NaYF_4$ nanoparticles and three recognized efficient nanostructures under different excitation models (*i.e.* $NaYF_4$:20% Yb,2%

‡During the preparation of this manuscript, a related work on $NaErF_4$@$NaLuF_4$ nanoparticle was reported (N. J. Johnson, S. He, S. Diao, E. M. Chan, H. J. Dai and A. Almutairi, *J. Am. Chem. Soc.*, 2017, DOI: 10.1021/jacs.7b00223. First published online 07 Feb 2017).

$Er@NaYF_4$:20%Yb@$NaYF_4$:10% Nd nanoparticles under the excitation of 800 nm,[16,27] $NaYF_4$:20% Yb,2% $Er@NaYF_4$ nanoparticles under the excitation of 980 nm (ref. 28 and 29) and $NaYF_4$:20% $Er@NaYF_4$ nanoparticles under the excitation of 1530 nm;[30,31] all the contrast samples have a similar structure with ~20 nm core and ~5 nm shell; refer to the ESI Fig. S2†). As shown in Fig. 2a–c, the UC emission intensity (especially the red emission band) of $NaErF_4@NaYF_4$ nanoparticles is at the same level (under 800 nm or 980 nm excitation) or even exceeds by an order (under 1530 nm excitation) that of its counterparts. And it is also worth noticing that, within the visible spectral range, the UC emission of the $NaErF_4@NaYF_4$ nanostructure always has a relatively high red/green (R/G) ratio (over 10, Fig. 2d). This characteristic can be attributed to the efficient cross relaxation (CR) interactions between up-closed Er^{3+},[31–34] *i.e.* CR_{800ex}: $2\ {}^4I_{9/2} \rightarrow {}^4S_{3/2} + {}^4I_{13/2}$ and ${}^4S_{3/2} + {}^4I_{9/2} \rightarrow 2\ {}^4F_{9/2}$, CR_{980ex}: ${}^4F_{7/2} + {}^4I_{11/2} \rightarrow 2\ {}^4F_{9/2}$ and CR_{1530ex}: ${}^4S_{3/2} + {}^4I_{9/2} \rightarrow 2\ {}^4F_{9/2}$ (Fig. 3b). Furthermore, utilizing the energy transfer between Er^{3+} and Tm^{3+}, we determined that, through a feasible improvement strategy (introducing 0.5 mol% Tm^{3+} into the $NaErF_4$ core) to drive down the green emission,[35] the R/G ratio could be further enhanced to over 50, thus achieving efficient monochromic red emission (refer to the ESI Fig. S3†). To the best of our knowledge, this is the first time one type of UC material has achieved monochromic UC red emission under excitation with three different NIR wavelengths.

The unique properties of the $NaErF_4@NaYF_4$ nanostructures come from the following reasons. Firstly, the absorption ability of the nanoparticles increases to be comparable with the traditional sensitizer (Yb^{3+} or Nd^{3+}) co-doped nanoparticles due to the Er^{3+} concentration rising to 100 mol% (refer to the ESI Fig. S4†). Secondly, the strong UC emission of the $NaErF_4@NaYF_4$ nanoparticles suggests that the concentration quenching effect could be efficiently suppressed, which guides us in a re-consideration of the concentration quenching mechanism. In the traditional understanding, with the doping concentration increasing, the cascade energy migration and CR process between activators and/or sensitizers will be more and more efficient, thus leading to the excited states energy being more easily captured by the quenching sites in the system, and thereby quenching the UC emission.[15,36] However, there is still a blind spot in the consideration above: if the system is totally "quenching site free" (or the influence of quenching sites could be neglected), there will be no sites to dissipate the migrated excited state energy. What will happen? In our opinion, in that ideal case, the high mobility of the excited states (induced by the high concentration of activator) is actually harmless. It even benefits the UC efficiency by promoting the possibility of interaction between excited states (Fig. 3a), and therefore the concentration quenching effect could be completely eliminated in the "quenching site free" system. Herein, the $NaErF_4@NaYF_4$ core–shell nanostructure should be considered as a "quenching site free" system. For this system, firstly, because of its nano-sized characteristic, it is made up of only a few crystal lattices (compared with bulk material); thus it is entirely possible to form a luminescent core area without any quenching sites

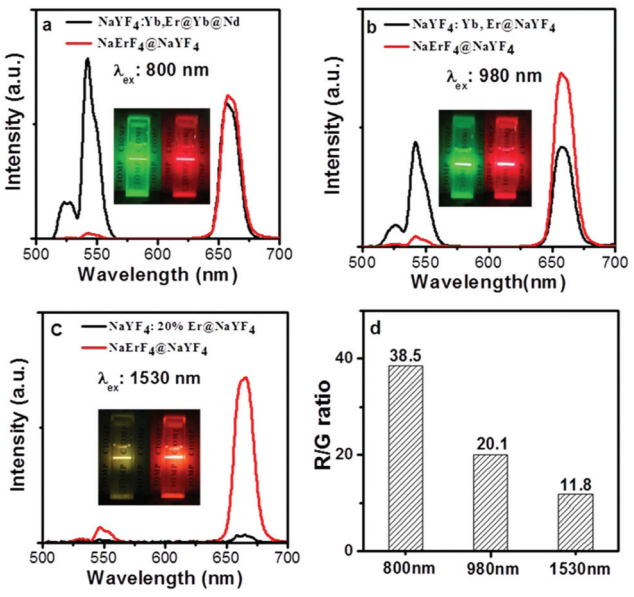

Fig. 2 UC emission spectra of cyclohexane solutions containing $NaErF_4@NaYF_4$ nanoparticles with the corresponding contrasts (a) 800 m excitation (10 W cm^{-2}), (b) 980 nm excitation (10 W cm^{-2}), (c) 1530 nm excitation (1 W cm^{-2}). Insets a–c: The luminescent photos of cyclohexane solutions containing $NaErF_4@NaYF_4$ (monochromic red emission) and its counterparts, respectively. (d) The R/G ratios (intensity) of $NaErF_4@NaYF_4$ nanoparticles under 800 nm, 980 nm and 1530 nm excitation, respectively.

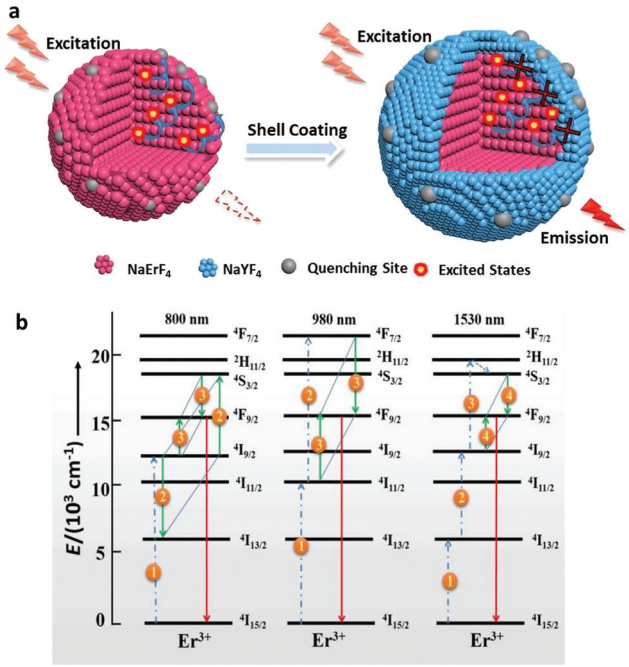

Fig. 3 (a) Schematic of the energy accumulation processes in bare core and core–shell nanostructures. (b) Energy level diagrams of Er^{3+} ions as well as proposed CR mechanisms in nanostructures under 800 nm, 980 nm and 1530 nm excitation, respectively.

inside. Secondly, by blocking the energy dissipation path from the luminescent core to the surface, the surface quenching sites of the nanoparticles could be deactivated by an inert shell ($NaYF_4$) coating. To verify our suggestion, we broke the ideal environment of the Er^{3+} by introducing quenching sites into the nanoparticles. As discussed in the ESI Fig. S5 and S6,† for either the $NaErF_4$ bare core (which contains lots of quenching sites on the surface) or $NaErF_4$:0.5% Nd^{3+}@$NaYF_4$ core–shell nanoparticles (where Nd^{3+} plays the role of bulk quenching sites), a deterioration in the concentration quenching effect occurred.

To further demonstrate our hypothesis that the concentration quenching effect could be controlled by the environment of the activator (*e.g.* surface quenching sites), a series of comparisons between Er^{3+} singly doped bare core ($NaYF_4$:*x*% Er^{3+}, *x*: 2–100) and core-inert shell ($NaYF_4$:*x*% Er^{3+}@$NaYF_4$, *x*: 2–100) nanoparticles have been conducted (Fig. 4). 980 nm excitation was taken as an example (similar results obtained with 800 nm and 1530 nm excitation are shown in ESI Fig. S7 and S8†). In the bare core structure, the optimal doping concentration of Er^{3+} is limited to 2–20 mol% (Fig. 4a), which is in good accord with previous reports,[31,34,37] and the Er^{3+} heavy-doped nanoparticles exhibit very weak UC emission (especially for the $NaErF_4$ bare core, where there is almost no UC emission at all). However, after the $NaYF_4$ shell coating, the optimal concentration is promoted to 100 mol% (Fig. 4b), and the brightest UC emission could be observed from the $NaErF_4$@$NaYF_4$ nanoparticles. These results indicate that in the bare core structure, the concentration quenching phenomenon is mainly induced by the energy dissipation from the activators to the surface quenching sites. Typically, with an increase in the doping concentration, the ion-to-ion distance decreases, thus leading to the more and more efficient energy migration and CR process between Er^{3+} ions. In the presence of numerous surface quenching sites, the efficient energy migration and CR process will be harmful to the UC emission by increasing the possibility of excited state energy being trapped by surface quenching sites.[38,39] On the other hand, the coated inert shell ($NaYF_4$) will block the crucial path of energy dissipation from the core area, thus completely eliminating the concentration quenching effect and raising the optimal doping concentration of Er^{3+} to 100 mol%. The time-resolved experimental results re-confirmed our hypothesis. In the bare core, due to the energy dissipation from the core to the particle surface, with the Er^{3+} doping concentration increased from 2 mol% to 100 mol%, the decay lifetime of 650 nm emission ($^4F_{9/2} \rightarrow {}^4I_{15/2}$) will be sharply shortened from 529 μs to 15.9 μs (Fig. 4c). After the shell coating, whatever the concentration of Er^{3+}, the energy dissipation from the core to the surface quenching sites will be inefficient, resulting in a relatively small change in the decay lifetime (shortened from 562 μs to 311 μs; refer to Fig. 4d).

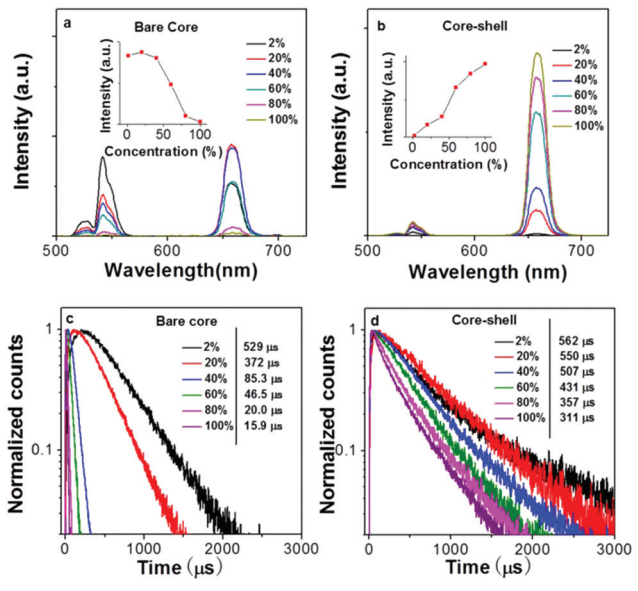

Fig. 4 The UC emission spectra of (a) $NaYF_4$:*x*% Er (*x*: 2–100) bare core, (b) $NaYF_4$:*x*% Er (*x*: 2–100)@$NaYF_4$ core–shell nanoparticles (in cyclohexane, normalized by the number of nanoparticles, excited by 980 nm): inserts: Er^{3+} concentration dependent UC emission intensity (integration from 500 nm to 700 nm) in bare core and core–shell structure, respectively. (c) The decay curves of Er^{3+}: $^4F_{9/2} \rightarrow {}^4I_{15/2}$ transition (~650 nm) in the bare core nanostructure and (d) the decay curves of Er^{3+}: $^4F_{9/2} \rightarrow {}^4I_{15/2}$ transition (~650 nm) in the core–shell nanostructure.

Obviously, the unique properties of the core–shell nanostructures will shed light on many potential applications of UC materials in fields like biology, display, solar cells and anti-counterfeiting. In the following work, two typical applications are performed. Firstly, we examined its high potential in solar energy utilization. In this field, UC materials have the potential to convert NIR to UV/VIS light to enhance the utilization of the solar spectrum.[40–42] Compared with traditional UC materials, the $NaErF_4$@$NaYF_4$ nanostructure is privileged to convert three different NIR bands simultaneously rather than only one. More importantly, due to the non-linear relationship existing between the excitation power and UC emission intensity (refer to the ESI Fig. S9†),[43] the energy conversion efficiency will increase sharply when the multi-bands excitation effects are superimposed. This characteristic is demonstrated by a proof-of-concept experiment.

As shown in Fig. 5, we constructed an experiment with three continuous wavelength (CW) lasers so that the excitation manipulation and assembly of the beams can be well controlled. To obtain a direct comparison, we first recorded the emissions under single laser excitation and ensured that their intensities were close to the same level. Then the cooperative excitation of three lasers (800 nm, 980 nm and 1530 nm) was conducted, and the obtained emission spectra are shown in Fig. 5. We observed that the UC emission intensity from cooperative excitation (pink curve) was 6.1 times higher than the UC emission by single laser excitation (*i.e.* the coincident black, red, and blue curves). It should be noted that the calculated linear sum of emissions only reached 3 times higher (green curve). This result has robustly demonstrated that the new structure is superior to traditional UC nanoparticles in the field of solar energy utilization.

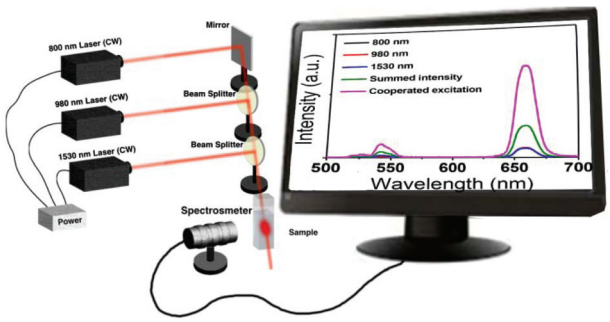

Fig. 5 Schematic illustration of experimental setup for cooperative excitation with three CW lasers at 800 nm, 980 nm and 1530 nm. And the measured UC emission spectra of $NaErF_4$@$NaYF_4$ nanostructures under 800 nm, 980 nm, 1530 nm and cooperative excitation with these three CW lasers, respectively.

Secondly, since the Ln^{3+} doped UC material has the advantages of photostability, zero-background and unique anti-Stokes emission, it is also believed to be a promising material for anti-counterfeiting.[44,45] Obviously, high-level confidentiality depends on the diversity and selectivity of the excitation and emission wavelength, and thus the $NaErF_4$@$NaYF_4$ nanoparticles can be regarded as a proper candidate. As a proof of concept, triply encrypted characters can be achieved by the combination of three types of inks containing different UC materials (Ink I: $NaYF_4$:20%Yb,2%Er@$NaYF_4$:20%Yb@$NaYF_4$:10%Nd; Ink II: $NaYF_4$:20%Yb,2%Er@$NaYF_4$; Ink III: $NaErF_4$@$NaYF_4$). As shown in Fig. 6, we designed a triple encryption experiment by writing concealed information with different inks layer by layer. When excited at 980 nm, the green characters "8 9 8" appear and come from ink I to form coding information I. When the excitation wavelength shifts to 800 nm, ink II generates information II to replace the previous information, which appears to be the green characters "4 3 6". By introducing the new material $NaErF_4$@$NaYF_4$ as ink III, the security level is improved. As the excitation is altered to 1530 nm, the coding information III displays as red characters "1 7 5". It should be noted that under the 800 or 980 nm excitation, ink III also generates red UC emission. However, this emission will easily be covered by the green light induced by ink I or II since the human eye is more sensitive to the green light region.

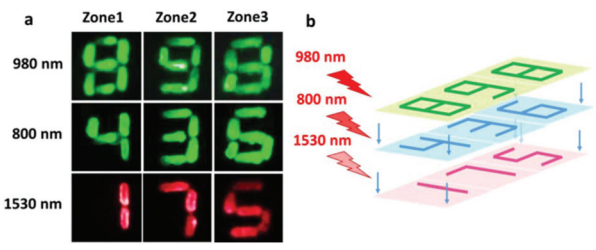

Fig. 6 (a) Represents the different characters observed under 980 nm, 800 nm and 1530 nm excitation, respectively. (b) Depicts the process and approach of preparing these characters layer by layer.

4. Conclusions

In summary, we indicate that the concentration quenching effect of Er^{3+} in a core-inert shell structure could be eliminated. The new finding enables us to set up an $NaErF_4$@$NaYF_4$ UC nanostructure and its relevant derivatives (*e.g.* $NaErF_4$:0.5% Tm@$NaYF_4$), which successfully achieve three highly desirable UC properties simultaneously: *i.e.* high efficiency, multi-band excitation (~800 nm, ~980 nm and 1530 nm) and monochromic red emission. Furthermore, by proof-of-concept experiments, we demonstrated the bright potential of this novel nanostructure in the applications of solar cells and anti-counterfeiting.

Acknowledgements

This work was financially supported by NSF of China (11374297, 61575194, 11674316, 11504371 and 11604331), Project of Science and Technology Agency, Jilin Province (20170520113 JH, 20170520112JH and 20170519002JH), Joint research program between CAS of China and KNAW of the Netherlands, European Union MSCA-ITN-2015-ETN Action program, ISPIC, under grant no. 675742 and Netherlands Organisation for Scientific Research in the framework of the Fund New Chemical Innovation (2015) TA under grant no. 731.015.206, EU COST program no. 1403 and HRSMC Research fellowship.

Notes and references

1 J. C. G. Bunzli, *Chem. Rev.*, 2010, **110**, 2729–2755.
2 F. Auzel, *Chem. Rev.*, 2004, **104**, 139–173.
3 J. Zhou, Z. Liu and F. Y. Li, *Chem. Soc. Rev.*, 2012, **41**, 1323–1349.
4 L. D. Sun, Y. F. Wang and C. H. Yan, *Acc. Chem. Res.*, 2014, **47**, 1001–1009.
5 G. Y. Chen, H. L. Qju, P. N. Prasad and X. Y. Chen, *Chem. Rev.*, 2014, **114**, 5161–5214.
6 C. Drees, A. N. Raj, R. Kurre, K. B. Busch, M. Haase and J. Piehler, *Angew. Chem., Int. Ed.*, 2016, **55**, 11668–11672.
7 B. Zhou, B. Y. Shi, D. Y. Jin and X. G. Liu, *Nat. Nanotechnol.*, 2015, **10**, 924–936.
8 H. Dong, S. R. Du, X. Y. Zheng, G. M. Lyu, L. D. Sun, L. D. Li, P. Z. Zhang, C. Zhang and C. H. Yan, *Chem. Rev.*, 2015, **115**, 10725–10815.
9 X. M. Li, F. Zhang and D. Y. Zhao, *Chem. Soc. Rev.*, 2015, **44**, 1346–1378.
10 P. Lederhose, Z. J. Chen, R. Muller, J. P. Blinco, S. Wu and C. Barner-Kowollik, *Angew. Chem., Int. Ed.*, 2016, **55**, 12195–12199.
11 W. Zheng, P. Huang, D. T. Tu, E. Ma, H. M. Zhu and X. Y. Chen, *Chem. Soc. Rev.*, 2015, **44**, 1379–1415.
12 X. S. Yang, H. Xie, E. Alonas, Y. J. Liu, X. Z. Chen, P. J. Santangelo, Q. S. Ren, P. Xi and D. Y. Jin, *Light: Sci. Appl.*, 2016, **5**, 8.

13 M. Haase and H. Schafer, *Angew. Chem., Int. Ed.*, 2011, **50**, 5808–5829.
14 L. P. Tu, X. M. Liu, F. Wu and H. Zhang, *Chem. Soc. Rev.*, 2015, **44**, 1331–1345.
15 G. Y. Chen, C. H. Yang and P. N. Prasad, *Acc. Chem. Res.*, 2013, **46**, 1474–1486.
16 Y. T. Zhong, G. Tian, Z. J. Gu, Y. J. Yang, L. Gu, Y. L. Zhao, Y. Ma and J. N. Yao, *Adv. Mater.*, 2014, **26**, 2831–2837.
17 W. Wei, G. Y. Chen, A. Baev, G. S. He, W. Shao, J. Damasco and P. N. Prasad, *J. Am. Chem. Soc.*, 2016, **138**, 15130–15133.
18 X. M. Liu, X. G. Kong, Y. L. Zhang, L. P. Tu, Y. Wang, Q. H. Zeng, C. G. Li, Z. Shi and H. Zhang, *Chem. Commun.*, 2011, **47**, 11957–11959.
19 J. Wang, R. R. Deng, M. A. MacDonald, B. L. Chen, J. K. Yuan, F. Wang, D. Z. Chi, T. S. A. Hor, P. Zhang, G. K. Liu, Y. Han and X. Liu, *Nat. Mater.*, 2014, **13**, 157–162.
20 J. B. Zhao, D. Y. Jin, E. P. Schartner, Y. Q. Lu, Y. J. Liu, A. V. Zvyagin, L. X. Zhang, J. M. Dawes, P. Xi, J. A. Piper, E. M. Goldys and T. M. Monro, *Nat. Nanotechnol.*, 2013, **8**, 729–734.
21 D. J. Gargas, E. M. Chan, A. D. Ostrowski, S. Aloni, M. V. P. Altoe, E. S. Barnard, B. Sanii, J. J. Urban, D. J. Milliron, B. E. Cohen and P. J. Schuck, *Nat. Nanotechnol.*, 2014, **9**, 300–305.
22 W. Wei, Y. Zhang, R. Chen, J. Goggi, N. Ren, L. Huang, K. K. Bhakoo, H. D. Sun and T. T. Y. Tan, *Chem. Mater.*, 2014, **26**, 5183–5186.
23 H. B. Wang, W. Lu, T. M. Zeng, Z. G. Yi, L. Rao, H. R. Liu and S. J. Zeng, *Nanoscale*, 2014, **6**, 2855–2860.
24 H. S. Qian and Y. Zhang, *Langmuir*, 2008, **24**, 12123–12125.
25 N. J. J. Johnson, A. Korinek, C. H. Dong and F. van Veggel, *J. Am. Chem. Soc.*, 2012, **134**, 11068–11071.
26 F. Wang and X. G. Liu, *Chem. Soc. Rev.*, 2009, **38**, 976–989.
27 D. Wang, B. Xue, X. G. Kong, L. P. Tu, X. M. Liu, Y. L. Zhang, Y. L. Chang, Y. S. Luo, H. Y. Zhao and H. Zhang, *Nanoscale*, 2015, **7**, 190–197.
28 F. Zhang, R. C. Che, X. M. Li, C. Yao, J. P. Yang, D. K. Shen, P. Hu, W. Li and D. Y. Zhao, *Nano Lett.*, 2012, **12**, 2852–2858.
29 X. M. Li, R. Wang, F. Zhang and D. Y. Zhao, *Nano Lett.*, 2014, **14**, 3634–3639.
30 S. Fischer, B. Frohlich, K. W. Kramer and J. C. Goldschmidt, *J. Phys. Chem. C*, 2014, **118**, 30106–30114.
31 G. Y. Chen, T. Y. Ohulchanskyy, A. Kachynski, H. Agren and P. N. Prasad, *ACS Nano*, 2011, **5**, 4981–4986.
32 F. Vetrone, J. C. Boyer, J. A. Capobianco, A. Speghini and M. Bettinelli, *Chem. Mater.*, 2003, **15**, 2737–2743.
33 F. Liu, E. Ma, D. Q. Chen, Y. L. Yu and Y. S. Wang, *J. Phys. Chem. B*, 2006, **110**, 20843–20846.
34 X. Y. Shang, P. Chen, T. Q. Jia, D. H. Feng, S. Zhang, Z. R. Sun and J. R. Qiu, *Phys. Chem. Chem. Phys.*, 2015, **17**, 11481–11489.
35 E. M. Chan, G. Han, J. D. Goldberg, D. J. Gargas, A. D. Ostrowski, P. J. Schuck, B. E. Cohen and D. J. Milliron, *Nano Lett.*, 2012, **12**, 3839–3845.
36 J. F. Suyver, J. Grimm, M. K. van Veen, D. Biner, K. W. Kramer and H. U. Gudel, *J. Lumin.*, 2006, **117**, 1–12.
37 R. Martin-Rodriguez, S. Fischer, I. Aruna, B. Froehlich, K. W. Kramer, J. C. Goldschmidt, B. S. Richards and A. Meijerink, *Chem. Mater.*, 2013, **25**, 1912–1921.
38 B. Zhou, L. L. Tao, Y. Chai, S. P. Lau, Q. Y. Zhang and Y. H. Tsang, *Angew. Chem., Int. Ed.*, 2016, **55**, 12356–12360.
39 T. Y. Sun, R. H. Ma, X. S. Qiao, X. P. Fan and F. Wang, *ChemPhysChem*, 2016, **17**, 766–770.
40 Z. Chen, G. B. Wu, H. Jia, K. Sharafudeen, W. B. Dai, X. W. Zhang, S. F. Zeng, J. M. Liu, R. F. Wei, S. C. Lv, G. P. Dong and J. R. Qiu, *J. Phys. Chem. C*, 2015, **119**, 24056–24061.
41 S. Fischer, E. Favilla, M. Tonelli and J. C. Goldschmidt, *Sol. Energy Mater. Sol. Cells*, 2015, **136**, 127–134.
42 M. He, X. C. Pang, X. Q. Liu, B. B. Jiang, Y. J. He, H. Snaith and Z. Q. Lin, *Angew. Chem., Int. Ed.*, 2016, **55**, 4280–4284.
43 M. Pollnau, D. R. Gamelin, S. R. Luthi, H. U. Gudel and M. P. Hehlen, *Phys. Rev. B: Condens. Matter*, 2000, **61**, 3337–3346.
44 K. Huang, N. M. Idris and Y. Zhang, *Small*, 2016, **12**, 836–852.
45 Y. H. Zhang, L. X. Zhang, R. R. Deng, J. Tian, Y. Zong, D. Y. Jin and X. G. Liu, *J. Am. Chem. Soc.*, 2014, **136**, 4893–4896.